



**HAL**  
open science

## Evaluation of a scattering correction method for high energy tomography

D. Tisseur, N. Bhatia, N. Estre, L. Berge, D. Eck, E. Payan

► **To cite this version:**

D. Tisseur, N. Bhatia, N. Estre, L. Berge, D. Eck, et al.. Evaluation of a scattering correction method for high energy tomography. International conference on advancements in nuclear instrumentation measurement methods and their applications, Jun 2017, Liege, Belgium. hal-02417730

**HAL Id: hal-02417730**

**<https://hal.science/hal-02417730>**

Submitted on 18 Dec 2019

**HAL** is a multi-disciplinary open access archive for the deposit and dissemination of scientific research documents, whether they are published or not. The documents may come from teaching and research institutions in France or abroad, or from public or private research centers.

L'archive ouverte pluridisciplinaire **HAL**, est destinée au dépôt et à la diffusion de documents scientifiques de niveau recherche, publiés ou non, émanant des établissements d'enseignement et de recherche français ou étrangers, des laboratoires publics ou privés.

# Evaluation of a scattering correction method for high energy tomography

David Tisseur, Navnina Bhatia, Nicolas Estre, Léonie Berge, Daniel Eck, Emmanuel Payan

**Abstract**—One of the main drawbacks of Cone Beam Computed Tomography (CBCT) is the contribution of the scattered photons due to the object and the detector. Scattered photons are deflected from their original path after interaction with the object. This additional contribution of the scattered photons results in increased measured intensities, since the scattered intensity simply adds to the transmitted intensity. This effect is seen as an overestimation in the measured intensity thus corresponding to an underestimation of absorption. This results in artifacts like cupping, shading, and streaks etc. on the reconstructed images. Moreover, the scattered radiation provides a bias for the quantitative tomography reconstruction (for example atomic number and volumic mass measurement with bi-energy technique). The effect can be significant and difficult in the range of MeV energy using large objects due to higher Scatter to Primary Ratio (SPR). Additionally, the incident high energy photons which are scattered by the Compton effect are more forward directed and hence more likely to reach the detector. Moreover, for MeV energy range, the contribution of the photons produced by pair production and Bremsstrahlung process also becomes important. We propose an evaluation of a scattering correction technique based on the method named Scatter Kernel Superposition (SKS). The algorithm uses a continuously thickness-adapted kernels method. The analytical parameterizations of the scatter kernels are derived in terms of material thickness, to form continuously thickness-adapted kernel maps in order to correct the projections. This approach has proved to be efficient in producing better sampling of the kernels with respect to the object thickness. This technique offers applicability over a wide range of imaging conditions and gives users an additional advantage. Moreover, since no extra hardware is required by this approach, it forms a major advantage especially in those cases where experimental complexities must be avoided. This approach has been previously tested successfully in the energy range of 100 keV – 6 MeV. In this paper, the kernels are simulated using MCNP in order to take into account both photons and electronic processes in scattering radiation contribution. We present scatter

correction results on a large object scanned with a 9 MeV linear accelerator.

**Index Terms**— Computed tomography, scatter correction, Scatter Kernel Superposition

## I. INTRODUCTION

One of the main drawbacks of MeV energy range CBCT is scattering of photons inside the object and the detector. Scattered photons intensity is simply added to the primary photons intensity. This effect is seen in the back projection reconstruction algorithms as overestimated reconstructed linear attenuation thus corresponding to an underestimation of absorption. As a result, scatter artifacts can be seen on the reconstruction images like cupping, shading, streaks etc. In case of MeV energy range, forward Compton scattering of photons increases and hence there is a high probability of scattered photons reaching the detector. In addition, these scattered photons are more energetic and therefore more likely to escape from the object. Moreover, when the incident X-ray energy range is increased, the number of photons generated by the bremsstrahlung process also increases. Finally, for the X-ray photons with energies above 1.022 MeV, pair production produces additional 511 keV photons that can contribute to an overall increase in the scatter contribution. Many scatter correction methods for MeV source are listed in the literature. For example, Maltz et al. [1] have used beam stop arrays for scatter correction. Such methods increase the X-ray exposure due to more than one scan per projection and extended scanning time. The classical convolution approaches based on scatter kernel superposition (SKS) method [2] [3] [4] use deconvolution method to calculate the scatter intensity and are based on a discrete set of thickness-dependent kernels. In these techniques, for a range of thickness only one kernel is used. These methods give satisfactory results in many applications. However, these methods are not very efficient in higher energy range due to higher SPR. In this article, we have applied scatter correction by continuously thickness adapted Scatter Kernel Superposition (SKS) method [5] on a data produced by 9 MeV X-ray photon beam generated from a linear accelerator.

## II. METHOD AND MATERIALS

### A. Scatter correction using a continuous SKS approach

In the SKS scatter correction approach based on [5], scatter signal is modeled as the sum of the scatter contributions from

David Tisseur, Nicolas Estre, Léonie Berge, Daniel Eck and Emmanuel Payan are with the CEA Cadarache DEN/Nuclear Measurement Laboratory, F-13108 Saint-Paul lez Durance, France (e-mail: [david.tisseur@cea.fr](mailto:david.tisseur@cea.fr)). Navnina Bhatia works at Imagopole – Citech Institut Pasteur, Paris, France and has performed her Ph.D at CEA (2013-2016).

a group of pencil beams passing through the object and the detector. The total scatter signal  $S(m, n)$  with  $m$  and  $n$  as the pixel position on the detector, can then be modeled as:

$$S(m, n) = \sum_k \sum_l P(k, l) K_{T(k,l)}(m - k, n - l) \quad (1)$$

Where,  $P$  is the primary signal contributed by the photons passing through the object without any attenuation.  $K_T$  is the transmission ( $T$ ) dependent kernel, with amplitude equal to the ratio of the scattered signal at the current pixel to the primary signal  $P$ .  $T$  is computed with Beer Lambert law:

$$T(k, l) = \frac{P(k, l)}{O(k, l)} \quad (2)$$

Where,  $O$  is the full beam intensity (signal without the sample).  $T$  is dependent the attenuation thickness with respect to the classical Beer Lambert law.  $K_T$  is non-linearly fitted by an equation formed by a circularly symmetric Lorentzian function describing the shape of the kernel:

$$K_T(m - k, n - l) = \frac{A}{1 + B((m - k)^2 + (n - l)^2)} \quad (3)$$

Where parameters  $A, B$  are function of transmission  $T$ .

### B. Kernel generation with MNCNP6

In order to generate the kernels, we performed Monte Carlo (MC) simulations with MCNP6 [6]. Fig. 1 presents MC simulation setup and an example of the 2D kernel. Simulated geometry was kept same as the acquisition set up. Pencil beam source corresponding to a 9 MeV bremsstrahlung spectrum was impinged on slabs of the same material as the object under study. Afterwards, a discrete set of point spread 2D kernels was obtained on the detector.

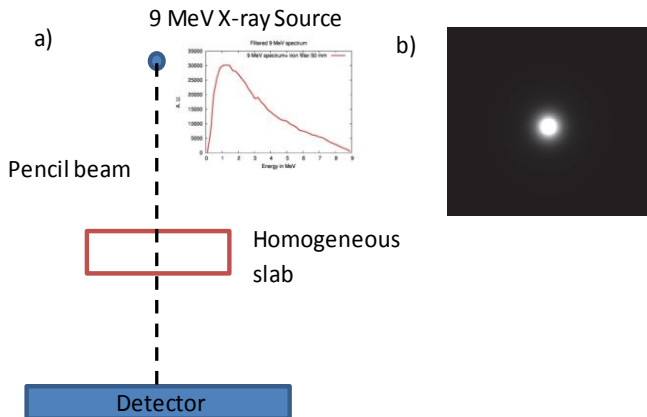


Fig. 1. a) MC kernel simulation setup using pencil beam b) generated 2D kernel

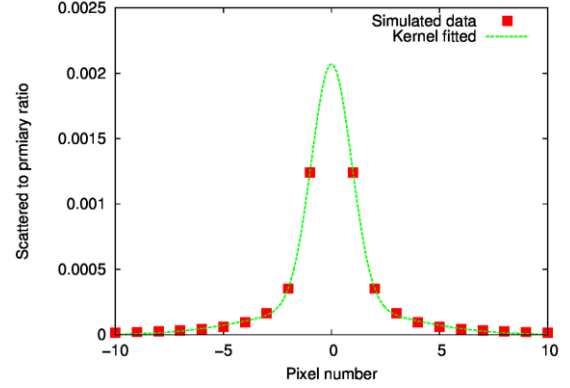


Fig. 2. Simulated and fitted kernel for bitumen slab of 45 cm. Eventually, for each kernel, we extracted a radial line profile from the 2D generated kernel image. Then, equation 3 was fit on these 1D kernels using non-linear least square fitting (see Fig. 2 and 3). The values for parameters  $A, B, \sigma_1, \sigma_2$  were calculated for these discrete sets of kernels. Thereupon, in order to obtain the continuous kernel, we analytically computed the expression for the kernels parameters  $A, B, \sigma_1, \sigma_2$  in terms of the transmission of the object [5]. For this case, we fitted a curve with respect to the transmission using a classical non linear least square fitting technique for each parameter. Fig. 3 presents the curve fitted on the discrete values of parameter  $A$  versus transmission.

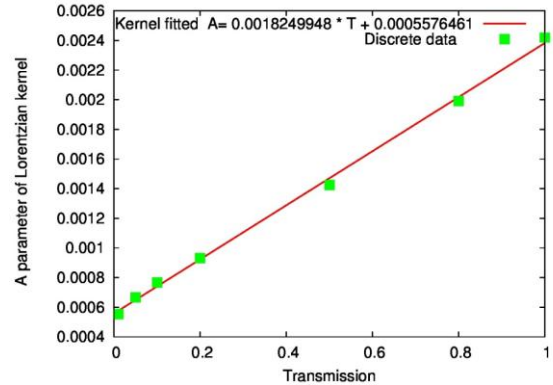


Fig. 3. Curve fitted on the discrete values of parameter  $A$  versus transmission

### C. Iterative Scatter Correction

We applied an iterative scatter correction scheme described in Fig. 4. It consists of 5 steps:

- 1) The experimental projection was initialized as the first estimate of the primary  $P$ .
- 2) The equivalent transmission was computed for each pixel using eq. (2).
- 3) The convolution was performed by calculating the suitable kernels for the respective transmission using eq. (3)
- 4) For each pixel, scatter contribution is estimated using eq. (1).
- 5) The primary  $P$  for iteration  $i+1$  was updated using eq. (4)

$$P_{i+1}(m, n) = P_0(m, n) \times \frac{P_i(m, n)}{P_i(m, n) + S_i(m, n)} \quad (4)$$

Steps 1 to 5 are repeated until convergence is achieved.

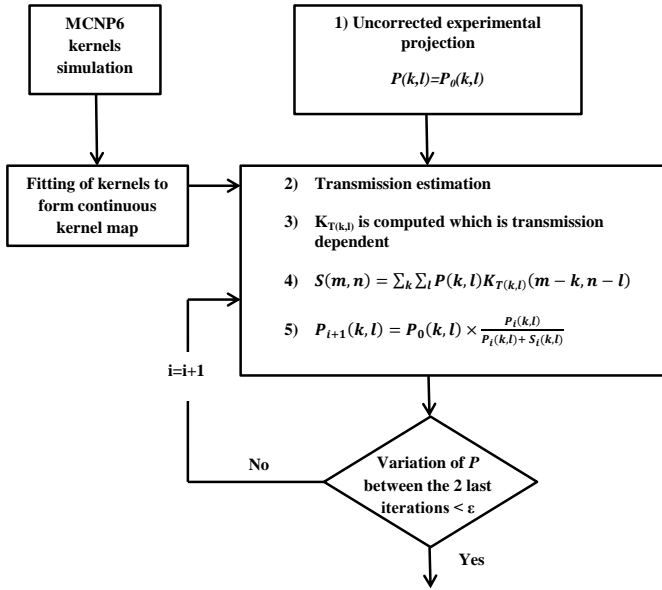


Fig. 4. Scatter correction synopsis

### D. Acquisition set up

The acquisitions were performed on a Mini-Linatron VARIAN linear accelerator 9 MeV filtered by 20 mm steel. The source to detector distance was 3.5 m and the source to object distance was 2.85 m. The acquisitions were performed on a cylinder made of bitumen. The detector used was a GADOX scintillator + sCMOS detector. Each of the 1200 projections over 360° have a size of 80 x 60 cm<sup>2</sup> with a pixel size of 334 μm (see Fig. 5).



Fig. 5. 2D scintillator detector. The scintillator screen is imaged by a low noise camera through a 45° tilted mirror. The screen size is 80 x 60 cm<sup>2</sup>.

### III. RESULTS

Fig. 6 shows one of 1200 projections acquired on the object presented at fig. 6 with our set up. The sample consisted of a bitumen cylinder with a diameter of around 400 mm containing steel bars. Outside the cylinder, we put some calibration material made of aluminum, silicon oxide, magnesium and water.

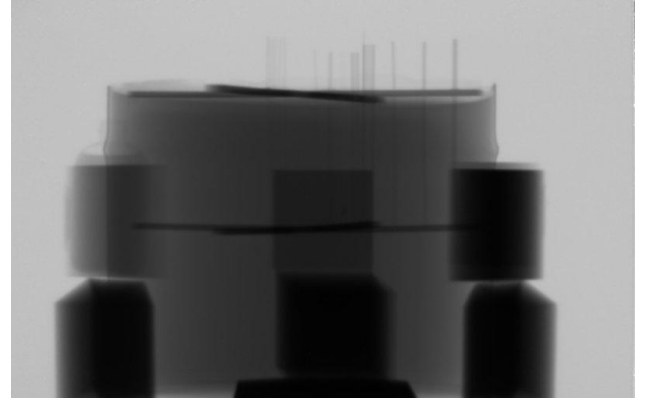


Fig. 6. Example of projection acquired on the set up

Scatter correction on the projections was applied using continuously adapted kernels described in Fig. 4. The reconstructions were performed on the uncorrected and corrected projections using FDK algorithm available in the Reconstruction Toolkit (RTK) [7]. Fig. 7 displays a reconstruction slice obtained with the corrected projections.

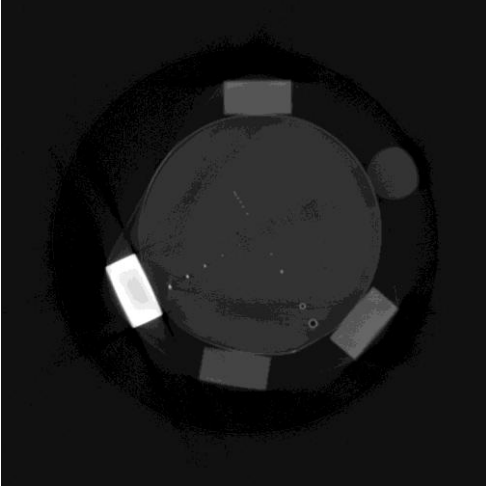


Fig.7. Example of a reconstruction slice.

TABLE I  
LINEAR ATTENUATION CM-1 VALUE COMPARISON WITH AND WITHOUT  
SCATTER CORRECTION

	theory	uncorrected	corrected
Magnesium	0.053	0.043	0.047
Aluminium	0.081	0.066	0.072
Water	0.032	0.028	0.033
Silicon	0.071	0.061	0.066

For each of the four calibration materials, we can compare the linear attenuation coefficient obtained after FDK tomographic reconstruction. The scatter correction results are compared at Table 1. For each of the 4 material, scatter correction improved the results. The gap between the theoretical value and the uncorrected value for aluminum, silicon, magnesium and water is respectively 17.7 %, 18.3%, 12.2% and 13.3 %. After scatter correction, the gap is respectively 11.2%, 10.8 %, 2.4% and 6.1 %.

#### IV. CONCLUSIONS

Scatter kernel were simulated accurately with MCNP6 to take into account both photonic and electronic processes in the considered energy range. Improvement in the quantitative reconstruction values for a heterogeneous and strongly attenuating object like the bitumen cylinder was obtained. The relative error between the obtained reconstruction value and the true value was reduced on average from 15.4 % to 6.4 %.

#### REFERENCES

[1] J. S. Maltz, B. Gangadharan, M. Vidal, A. Paidi, S. Bose, B. A. Faddego, M. Aubi, O. Morin, J. Pouliot, Z. Zheng, M. M. Svatos, and A. R. Bani-Hashemi. "Focused beam-stop array for the measurement of scatter in megavoltage portal and cone beam CT imaging.", *Med Phys*, 35(6):2452–2462, 2008.

[2] S. F. Petit, W. Elmpt, S. Nijsten, A. Dekker, and P. Lambin. "Correction of cupping artifacts in megavoltage cone beam computed tomography", Department of Radiation Oncology (MAASTRO), Masters thesis.

[3] M. Sun and J. M. Star-Lack. "Improved scatter correction using adaptive scatter kernel superposition", *Phys Med. Biol*, 55(22):6675 – 6720, 2010.

[4] V. N. Hansen, W. Swindell, and P. M. Evans. "Extraction of primary signal from EPIDs using only forward convolution". *Med. Phys.*, 24(49):1477–1484, 1997.

[5] N. Bhatia, D. Tisseur, F. Buyens, and J. M. Létang, "Scattering correction using continuously thickness-adapted kernels", *NDT & E*, 78:52–60, 2016.

[6] J.T. Goorley, et al., "Initial MCNP6 Release Overview – MCNP6 Version 1.0", Los Alamos National Laboratory Report, LA-UR-13-22934 (2013).

[7] S. Rit , M. Vila Oliva, S. Brousmiche, R. Labarbe, D. Sarrut, G.C. Sharp, "The Reconstruction Toolkit (RTK), an open-source cone-beam CT reconstruction toolkit based on the Insight Toolkit (ITK)" *Journal of Physics: Conference Series*, 489, 012079. doi:10.1088/1742-6596/489/1/012079 (2014)